Available online at www.sciencedirect.com

ScienceDirect

IFAC Papers Online CONFERENCE PAPER ARCHIVE

IFAC-PapersOnLine 49-23 (2016) 199–206

# Vision Restricted Path Planning and Control for Underactuated Vehicles

**Albert Sans-Muntadas, Kristin Y. Pettersen and Edmund Brekke**

*Centre for Autonomous Marine Operations and Systems (AMOS)*
*Department of Engineering Cybernetics at NTNU, NO-7491*
*Trondheim, Norway. E-mail: [albert.sans, kristin.y.pettersen, edmund.brekke]@itk.ntnu.no*

**Abstract:** Autonomous vehicles can obtain navigation information by observing a source with a camera or an acoustic system mounted on the frame of the vehicle. This information properly fused provides navigation information that can overcome the lack of other sources of positioning. However, these systems often have a limited angular field-of-view (FOV). Due to this restriction, motion along some paths will make it impossible to obtain the necessary navigation information as the source is no longer in the vehicle's FOV. This paper proposes both a path planning approach and a guidance control law that allows the vehicle to preserve a certain object or feature inside the FOV while at the same time converging to the proposed path.



*Keywords:* FOV Constraint, Landmark Navigation, Path Planning, Guidance, Underactuated Vehicle

## 1. INTRODUCTION

One of the challenges that autonomous vehicles face is navigating in environments where information from the global positioning system (GPS) is not available. This is a challenge that affects vehicles and systems that operate indoors, inside mines, or underwater. An alternative to the GPS is often computer vision or acoustic systems.

Although computer vision and acoustic systems have proven to be able to produce accurate information, they sometimes rely on a single source of information, either because camera information tracks only a single visual landmark, or because there is only a single node available of an acoustic network. In such cases the ability to navigate depends on the constant observation of the source.

Unfortunately the sensors receiving these signals are often limited by the FOV, an angular restriction to observe the target. In some configurations the sensors have the ability to change their direction and therefore partially overcome this limitation (Stolle and Rysdyk (2003); Rysdyk (2006)). Other setups may instead have these sensors fixedly attached to the vehicle's frame and then the observability of the target becomes dependent on the vehicle's trajectory. This restriction make some paths blinded because by following them the vehicle loses vision of the target. (See Fig.1) In some setups this can compromise the navigation capabilities of the vehicle. The path planning problem thus becomes more challenging, as it should not only find a feasible collision-free path to connect the start and end points but also preserve the view of the target. This restriction is often referred as the field-of-view constraint. In Boyadzhiev (1999); Tucker (2000) it is observed that

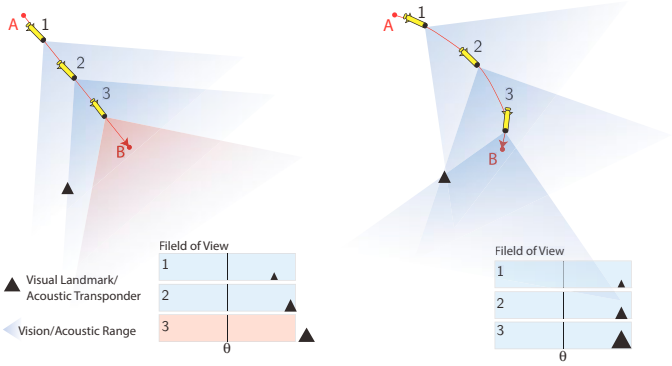


Fig. 1. Illustrative example of how two different paths can affect the observability of a target (▲) based on the FOV.

certain animals moving with respect to prey or a light source, follow a logarithmic spiral. This kind of spiral enables them to maintain the prey or light source in their field-of-view at all time during their motion. The existence of such trajectories in nature have inspired solutions to the FOV constraint. A formal definition of FOV is defined in Bhattacharya et al. (2007), where following a similar approach as the Reeds-Sheep car (Reeds and Shepp (1990)) describes a combination of straight lines and vision saturated curves that connect any two points in the plane. Later the optimal combination of trajectories is found and proven by Salaris et al. (2010). This work is further extended by Salaris et al. (2012) for side facing sensors.

Maniatopoulos et al. (2013) proposes a control law that guides the vehicle towards a desired point by using model predictive control (MPC). In López-Nicolás et al. (2010); Salaris et al. (2011) different control schemes are proposed to follow the optimal path with an underactuated robot that can turn on the spot.

⋆ This work was partly supported by the Research Council of Norway through the Centers of Excellence funding scheme, project No. 223254 AMOS, and project No. 205622.


10.1016/j.ifacol.2016.10.343

A common approach for path following control of underactuated vehicles is also the line-of-sight (LOS) guidance (Fossen (2011); Healey and Lienard (1993); Breivik et al. (2008)). The LOS guidance approach has the advantage of being simple and has a very small computational load (Fossen et al. (2015)). This guidance law was also generalized for curved paths in Børhaug and Pettersen (2006) using a Serret-Frenet frame and extended to handle currents in Moe et al. (2014). However, the different versions of LOS guidance and its variants do not deal with restrictions in the FOV.

The path planning and path following problems with the FOV constraint are tackled in two steps in this paper. The first step is the design of a path by using logarithmic spiral paths, which are a particular type of trajectories that appear as general solutions in FOV problems being discussed in López-Nicolás et al. (2010); Salaris et al. (2012); Bhattacharya et al. (2007); Salaris et al. (2010). The second step is a guidance and path following control law for underactuated vehicles which is an extension of LOS guidance laws. This control law is specifically designed to follow the logarithmic spirals generated in the first step, and in addition it ensures that the vehicle's maneuvers preserve the view of the target. Compared to Salaris et al. (2011) the proposed solution trades some optimality in path length for the sake of robustness. Furthermore, since underactuated vehicles are considered as opposed to mobile robots, the vehicles are only allowed to move in the forward direction, avoiding zero velocity which would make the vehicle uncontrollable. By using Lyapunov theory we prove that the proposed guidance control law makes the vehicles converge to the path. In particular, we prove that the closed-loop error dynamics are globally asymptotically stable.

The paper is organized as follows: In Section II we propose a logarithmic spiral that connects two points with a path along which the landmark/transponder is kept within the vehicle's FOV. In Section III, we discuss the Serret-Frenet frame, a relative frame that moves along this path, and which is used in order to describe the guidance control law and examine the stability properties. Section VI formalizes the control objectives and describes the proposed guidance and control system. Section VII examines the stability properties of the closed-loop system and Section VIII simulates the behavior of the system for two cases: a ground vehicle and an underwater vehicle.

## 2. VISION PRESERVING PATH

The first objective of this section is to describe the reachable set of points $\Gamma \in \mathbb{R}^2$ that can be connected with at least one path, for an underactuated vehicle that moves only with forward velocity, and the motion restricted by a FOV.

The start point of this path is denoted $\boldsymbol{p}_k$, and the path should satisfy the condition that during the whole path a certain target: (▲) (landmark/transponder) must be preserved inside the FOV. When the set of reachable points $\Gamma$ is defined, the next goal is to mathematically describe a vision preserving path that connects the starting point point $\boldsymbol{p}_k$ to another point $\boldsymbol{p}_{k+1} \in \Gamma$.

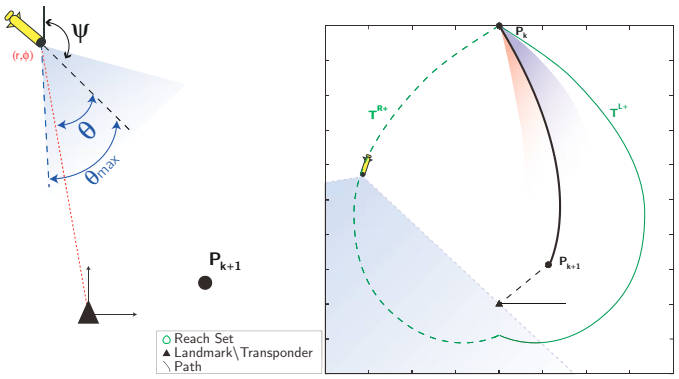


Fig. 2. On the left a representation of the FOV restriction: the angle $\theta$ the between the vehicle centerline and the target (▲) should be kept within the FOV boundary $\theta_{\max}$. The right figure shows the limit trajectories $T^{R+}, T^{L+}$ along which the target (▲) is always at the FOV limit. The region inside the boundaries $T^{R+}, T^{L+}$ contains the reachable set, and the black path is the proposed logarithmic-spiral trajectory.

The field-of-view is a solid angle in which a sensor can operate. Cameras and acoustic sensor tend to have this type of limitation. In this paper we assume that the origin of the earth-fixed coordinate system is defined at the landmark/transponder position. The objective is that the landmark/transponder is kept inside the FOV of the vehicle's sensor and can thus be expressed as follows:

*Condition 1.* $|\theta| \leqslant |\theta_{\max}| < \pi/2$

where $\theta$ is the bearing angle (See Fig. 2, left) between the vehicle centerline and the visual landmark/acoustic receiver.

For both objectives we assume:

*Assumption 1.* The FOV is forward looking, symmetric with maximum bearing $|\theta_{\max}| < \pi/2$ and aligned with the vehicle's centerline.

*Assumption 2.* The vehicle moves only with a forward speed $U$ where, $u_{\min} \leqslant u \leqslant u_{\max}$ and the sway speed $v$ is bounded by $|v| \leqslant v_{\max} < u_{\min}$.

This last is a necessary assumption for the path planning and control of underactuated vehicles, as they lose controllability when the velocity approaches zero.

### 2.1 Reach Set

In Salaris et al. (2010) the limit trajectories are described for a forward moving non-holonomic vehicle when the motion is restricted by the FOV. Such trajectories are logarithmic spirals and are also referred as: $T^{R+}$ and $T^{L+}$ (See Fig. 2 on the next page). These two trajectories represent the boundaries of the space that can be reached by a vehicle that only moves forward without violating the FOV restriction. These boundaries can also be expressed in a compact form as:

$$\Gamma_{P_p,\theta_{\max}} = \left\{ (r, \phi + \phi_p) | r = r_p e^{-\frac{|\phi|}{\tan(|\theta_{\max}|)}}, \phi \in [-\pi, \pi] \right\} \quad (1)$$

To reach any point at the boundary under the FOV restriction stated in Equation 1, the only possible trajectory is by

following a logarithmic-spiral. The rest of the points inside the boundaries, on the other hand, have endless combinations of possible trajectories. In Salaris et al. (2010) it was found that the optimal trajectory with respect to path length is a combination of straight lines ($S^+$) and limit spirals ($T^{R+}, T^{L+}$).

While this solution is optimal in terms of path length, it also requires the vehicle to move in such a way that the target (▲) is kept exactly at the boundaries of the FOV, and therefore any small disturbance making the vehicle drift outside the boundary, would make the target (▲) disappear from the field of view. It is for this reason that a suboptimal trajectory must be followed in order to achive a most robust control and always preserve the target (▲) inside the FOV. In this paper we thus propose a path that allows the vehicle to navigate safely within the boundaries.

### 2.2 Logarithmic Spirals

In this paper we propose to use logarithmic spirals to design a path that connects point $\boldsymbol{p}_k$ to point $\boldsymbol{p}_{k+1}$. Due to the nature of the problem, spirals are defined in polar coordinates where $r$ is the radius and $\phi$ is the angular coordinate. The logarithmic spiral path is parametrized by $\varpi \in [0,1]$, that connects $\boldsymbol{p}_k = (r_k, \phi_k)$ to point $\boldsymbol{p}_{k+1} = (r_{k+1}, \phi_{k+1})$ with a constant bearing angle.

$$\begin{aligned} r(\varpi) =& \varpi(r_{k+1} - r_k) + r_k \\ \phi(\varpi) =& \phi_k + \tan(\theta_k) \ln\left[\varpi(r_{k+1}/r_k - 1) + 1\right] \end{aligned} \tag{2}$$

where

$$\theta_k = \operatorname{atan}\left(\frac{\phi_{k+1} - \phi_k}{\ln(r_{k+1}/r_k)}\right) \tag{3}$$

This spiral-path has the distinctive property that it keeps the same bearing angle $\theta_k$ along the whole trajectory.

## 3. PATH PLANNING AND REFERENCE FRAME

In this section we transform the path equations into a tracking reference and use a relative frame that moves along the path, in order to later describe the guidance and control laws and examine the stability properties.

### 3.1 Path Description

The logarithmic Spiral described in the previous section will be used to describe the path to connect two waypoints $\boldsymbol{p}_k$ and $\boldsymbol{p}_{k+1}$. The position on this path will here be parameterized based on the distance traveled along the path, which is given by a parameter $s$. This will be used later in the control design as a tracking point $\boldsymbol{p}_f(s) = (r_f(s), \phi_f(s))$.

$$\begin{aligned} r_f(s) =& r_k - (s + s_0)\cos(\theta_k) \\ \phi_f(s) =& \phi_k + \tan(\theta_k) \ln\left(1 - \frac{(s + s_0)\cos(\theta_k)}{r_k}\right) \end{aligned} \tag{4}$$

where $s_0$ is a starting point that will be introduced later. The logarithmic spiral results from solving the differential equation:

$$\frac{r}{\frac{dr}{d\phi}} = \tan\theta_k \tag{5}$$

And the described path is among all the different possible logarithmic spirals that connect $\boldsymbol{p}_k$ and $\boldsymbol{p}_{k+1}$, the one with the smallest bearing angle $\theta_k$.

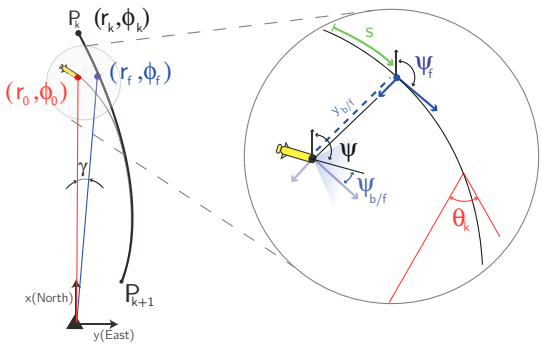


Fig. 3. The inertial frame (fixed at the landmark) $x$-axis points north and $y$-axis points east. The Serret-Frenet frame has axes denoted T and N. This frame is anchored to the desired path. The distance traveled along the path is described by $s$. The position of the body-fixed frame relative to the Serret-Frenet frame is denoted by $(x_{b/f}, y_{b/f})$

### 3.2 Serret-Frenet frame

The position of the vehicle is calculated relative to a frame that moves along the logarithmic spiral path parametrized by $s$ (see Fig.3), and in order to describe the dynamics of the vehicle with respect to this relative frame we use a Serret-Frenet frame. In this frame the relative position is denoted by $x_{b/f}, y_{b/f}$ and $\psi_{b/f} \triangleq \psi - \psi_f$ is the yaw angle relative to the frame (see similar approach in Moe et al. (2014) and Encarnaçao and Pascoal (2000)).

The kinematics of the body frame relative to the Serret-Frenet frame (Encarnaçao and Pascoal (2000)) can be described by the following the notation (Børhaug and Pettersen (2006)).

$$\begin{bmatrix} \dot{x}_{b/f} \\ \dot{y}_{b/f} \end{bmatrix} = \begin{bmatrix} \cos(\psi_{b/f}) & -\sin(\psi_{b/f}) \\ \sin(\psi_{b/f}) & \cos(\psi_{b/f}) \end{bmatrix} \begin{bmatrix} u \\ v \end{bmatrix} - \begin{bmatrix} \dot{s} \\ 0 \end{bmatrix} - \dot{s} \begin{bmatrix} 0 & -\kappa \\ \kappa & 0 \end{bmatrix} \begin{bmatrix} x_{b/f} \\ y_{b/f} \end{bmatrix} \tag{6}$$

In Figure 3 it can be seen that when $y_{b/f}$ goes to zero, this corresponds to the vehicle converging to the path.

*Assumption 3.* The difference $\gamma$ between the angular coordinate of the vehicle's position $\phi$ and the angular coordinate of the point on the Serret-Fernet $\phi_f(s)$ does not influence the limits of the FOV.

The reason for this assumption is because the guidance laws that ensure that the landmark/transponder is kept inside the FOV computes the desired yaw angle with respect to the angular coordinate of a point in the Serret-Frenet frame. This difference in the angular position of both could make the vehicle lose vision of the target if it becomes too large.

The following equation describes the distance from the current position of the vehicle to a point on the path:

$$d = r_0 + a^2 e^{-\frac{2\gamma}{\tan(\theta_k)}} - 2r_0 a e^{-\frac{\gamma}{\tan(\theta_k)}}\cos(\gamma) \tag{7}$$

where $a = r_k e^{-(\phi_0 - \phi_k)/\tan(\theta_k)}$. We find the point on the path closest to the vehicle's position by minimizing the distance $d$, i.e. solving $\frac{d}{d\gamma} d = 0$:

$$0 = -a e^{-\frac{\gamma}{\tan(\theta_k)}} + r_0\left[\cos(\gamma) + \sin(\gamma)\tan(\theta_k)\right] \tag{8}$$

With Assumption 3 the following approximations can be made:

$$\sin(\alpha) \approx \alpha; \quad \cos(\gamma) \approx 1; \quad e^{-\frac{\gamma}{\tan(\theta_k)}} \approx 1 - \frac{\gamma}{\tan(\theta_k)} \tag{9}$$

Solving for $\gamma$ in (8) we then find

$$\gamma^* \approx \tan(\theta_k) \frac{r_k e^{-\frac{\phi_0 - \phi_k}{\tan(\theta_k)}} - r_0}{r_0 \tan^2(\theta_k) + r_k e^{-\frac{\phi_0 - \phi_k}{\tan(\theta_k)}}} \tag{10}$$

Then the point of the path where we initialize the Serret-Frenet frame is:

$$s_0 = r_k \left(1 - e^{\frac{\phi_0 + \gamma^* - \psi_k}{\tan(\theta_k)}}\right) / \cos(\theta_k) \tag{11}$$

## 4. CONTROL OBJECTIVE AND CONTROL SYSTEM

The control objective is to make the vehicle converge to, and follow the logarithmic spiral path $\mathcal{C} = \{(x_f(s), y_f(s)\}$, defined by an initial point $\boldsymbol{p}_k$ and an endpoint $\boldsymbol{p}_{k+1}$. Based on the Serret-Frenet frame described in Section 3.2 the control objective is formalized as:

$$\begin{aligned} \lim_{t\to\infty} x_{b/f}(t) &= 0 \\ \lim_{t\to\infty} y_{b/f}(t) &= 0 \end{aligned} \tag{12}$$

We propose a yaw controller to guarantee convergence to the path, i.e. to fulfill the control objective (12), which can be divided in the following three components:

### *4.1 Serret-Frenet Frame update law*

The following equation describes the update law that will drive the Serret-Frenet frame along the path.

$$\dot{s} = u\cos(\psi_{b/f}) - v\sin(\psi_{b/f}) - k_x x_{b/f} \tag{13}$$

The first two terms are the projection of the vehicle forward velocity onto $x_{b/f}$. By doing so, the frame moves as fast as the vehicle in $x_{b/f}$ direction. Therefore, the velocity at which the frame moves along the path equals the velocity of the vehicle. This projection makes the guidance a path following problem where $y_{b/f}$ will determine the distance to the path. Based on that distance a guidance law will be derived in the next section. It is thus important that $x_{b/f}$ remains close to 0 because then the frame is located at the closest point to the vehicle. Since the first two terms regulate the speed of the vehicle, a third term $-k_x x_{b/f}$ is introduced, which acts as a restoring spring, ensuring the convergence to $x_{b/f} = 0$. This allows the update law to overcome errors in the initialization of $s_0$ or numerical errors caused by the integration of $s$, maintaining always $x_{b/f} = 0$.

### *4.2 Guidance Law*

The following guidance law is an extension of the well-known LOS guidance laws, and has been designed for underactuated vehicles that have no independent control input in the sideways direction. It commands a desired yaw angle that we will prove later that makes the system described by (6) converge to the desired path. In particular, this guidance law makes the vehicle converge to any path described by Eq. (4) and at the same time preserve the desired landmark/transponder (▲) inside the FOV.

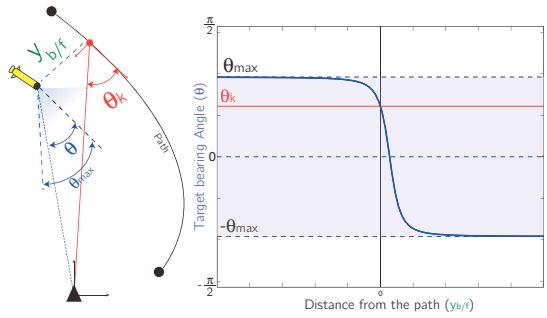


Fig. 4. Visualization of the behavior of the saturation controller. This prevents the trajectory to exceed the maximum field of vision defined by $\theta_{\max}$. It also offsets the function in order to guarantee the desired course when the vehicle is following the path.

$$\psi_d = \psi_f - \theta_k - \operatorname{atan}\left(\frac{v}{u}\right) \underbrace{- \operatorname{atan}\left(\frac{\tan(\theta_{\max})(y_{b/f} + d_{\theta_k})}{\sqrt{\Delta^2 + (y_{b/f} + d_{\theta_k})^2}}\right)}_{\text{Saturation controller}} \tag{14}$$

where $\Delta > 0$ is a design parameter inspired by the line-of-sight guidance method proposed by Papoulias (1991), $d_{\theta_k}$ is a shifting parameter that makes the heading angle at $y_{b/f} = 0$ the same as the desired constant path angle $\theta_k$ while $-\operatorname{atan}(v/u)$ compensates for the crab angle:

$$d_{\theta_k} = \Delta \tan(\theta_k) / \sqrt{\tan^2(\theta_{\max}) - \tan^2(\theta_k)} \tag{15}$$

Based on Assumption 3, the yaw controller described in Equation (14) does not consider the angle $\gamma$ between the angular coordinate of the tracking point on the Serret-Frenet frame and the angular coordinate of the vehicle's position.

### *4.3 Yaw controller*

The yaw dynamics of the vehicle can in general be written: (see. Fossen (2011)):

$$\begin{aligned} \dot{\psi} &= r \\ \dot{r} &= F_r(u, v, r) + \tau_r \end{aligned} \tag{16}$$

A feedback linearizing controller is used to follow the desired yaw angle $\psi_d$ provided by the guidance law (14):

$$\boldsymbol{\tau_r} = -\boldsymbol{F_r}(u, v, r) + \ddot{\psi}_d - k_\psi(\psi - \psi_d) - k_r(\dot{\psi} - \dot{\psi}_d) \tag{17}$$

where $k_\psi$ and $k_r$ are strictly positive constant controllers gains. From (16) and (17) it can be seen that it ensures exponential tracking. In particular, by defining $\tilde{\psi} = \psi - \psi_d$ and $\tilde{\dot{\psi}} = \dot{\psi} - \dot{\psi}_d$ and substituting the controller (17) into Equations (16), the yaw error dynamics can be written:

$$\dot{\boldsymbol{\xi}} = \begin{bmatrix} \dot{\tilde{\psi}} \\ \dot{\tilde{r}} \end{bmatrix} = \begin{bmatrix} 1 & 0 \\ k_\psi & k_r \end{bmatrix} \begin{bmatrix} \tilde{\psi} \\ \tilde{r} \end{bmatrix} = \boldsymbol{\Lambda\xi} \tag{18}$$

The system (18) is linear and time-invariant. Since the control parameters $k_\psi$ and $k_r > 0$, $\Lambda$ is Hurwitz and the origin $\boldsymbol{\xi} = 0$ is uniformly globally exponentially stable (UGES).

## 5. STABILITY ANALYSYS

The controller proposed in this paper allows an underactuated vehicle to follow a logarithmic spiral path while at the same time preserves vision of a target. In order to apply this controller on a large class of underactuated vehicles, the stability proof has been restricted only to the kinematic model. In order to prove the stability we redefine the expression of $\psi_{b/f} = \psi - \psi_f$:

$$\begin{aligned}\psi_{b/f} &= \tilde{\psi} + \psi_d - \psi_f \\ &= \tilde{\psi} - \theta_k - \operatorname{atan}\left(\frac{v}{u}\right) - \operatorname{atan}\left(\frac{\tan(\theta_{\max})(y_{b/f}+d_{\theta_k})}{\sqrt{\Delta^2+(y_{b/f}+d_{\theta_k})^2}}\right) \\ &= \tilde{\psi} - \theta_k - \underbrace{\operatorname{atan}\left(\frac{v\sqrt{\Delta^2+(y_{b/f}+d_{\theta_k})^2}+u\tan(\theta_{\max})(y_{b/f}+d_{\theta_k})}{u\sqrt{\Delta^2+(y_{b/f}+d_{\theta_k})^2}-v\tan(\theta_{\max})(y_{b/f}+d_{\theta_k})}\right)}_{\alpha}\end{aligned} \tag{19}$$

Based on the definition of $\alpha$ in equation 20, the expressions for $\sin(\alpha)$ and $\cos(\alpha)$ are:

$$\begin{aligned}\cos(\alpha) &= \frac{u\sqrt{\Delta^2+(y_{b/f}+d_{\theta_k})^2}-v\tan(\theta_{\max})(y_{b/f}+d_{\theta_k})}{\sqrt{U^2((\tan^2(\theta_{\max})+1)(y_{b/f}+d_{\theta_k})^2+\Delta^2)}} \\ \sin(\alpha) &= \frac{v\sqrt{\Delta^2+(y_{b/f}+d_{\theta_k})^2}+u\tan(\theta_{\max})(y_{b/f}+d_{\theta_k})}{\sqrt{U^2((\tan^2(\theta_{\max})+1)(y_{b/f}+d_{\theta_k})^2+\Delta^2)}}\end{aligned} \tag{20}$$

where $U = \sqrt{u^2+v^2}$.

Then substituting the update law (13), the controller (17) and the guidance law (14) into Equation (6) we obtain:

$$\dot{x}_{b/f} = -k_x x_{b/f} + \dot{s}\kappa\ y_{b/f} \tag{21}$$

$$\dot{y}_{b/f} = [\text{See exp. below}] \tag{22}$$

Equation (22) can be further reduced to (23) by using the expressions of $\sin(\alpha)$ and $\cos(\alpha)$ in (20). Then by using the coordinates of the yaw error dynamics defined in (18), the closed-loop system can be written as (18) together with:

$$\begin{bmatrix}\dot{x}_{b/f}\\ \dot{y}_{b/f}\end{bmatrix} = \begin{bmatrix}-k_x x_{b/f}\\ -U\frac{\tan(\theta_{\max})(y_{b/f}+d_{\theta_k})-\tan(\theta_k)\sqrt{\Delta^2+(y_{b/f}+d_{\theta_k})^2}}{\sqrt{\Delta^2+(1+\tan^2(\theta_k))(y_{b/f}+d_{\theta_k})^2/\cos(\theta_k)}}\end{bmatrix} - \dot{s}\begin{bmatrix}0 & -\kappa\\ \kappa & 0\end{bmatrix}\begin{bmatrix}x_{b/f}\\ y_{b/f}\end{bmatrix} + \boldsymbol{H}(U,\boldsymbol{\xi})\boldsymbol{\xi} \tag{24}$$

$$\boldsymbol{H}(U,\boldsymbol{\xi})\boldsymbol{\xi} = \begin{bmatrix}0 & 0\\ h(U,\boldsymbol{\xi}) & 0\end{bmatrix}\begin{bmatrix}\tilde{\psi}\\ \tilde{r}\end{bmatrix} \tag{25}$$

The system composed by Equations (18),(24) constitutes a cascaded system, where the nominal system (24) is perturbed by the exponentially stable error dynamics (18) through the interconnection term (25).

*Theorem 1.* Given an underactuated vehicle described by the dynamical system (6) and (16). If Assumptions 1-3 hold, then the update law (13), the guidance law (14) and the controller (17) guarantee the achievement of the control objectives (12).

Proof: To prove stability of the nominal part of (24) we choose the quadratic Lyapunov function candidate $V = \frac{1}{2}(x_{b/f}^2 + y_{b/f}^2)$. The derivative of $V$ is then obtained as:

$$\begin{aligned}\dot{V} &= \dot{x}_{b/f}x_{b/f} + \dot{y}_{b/f}y_{b/f} \\ &= \frac{\overbrace{-U\left[\tan(\theta_{\max})(y_{b/f}+d_{\theta_k})-\tan(\theta_k)\sqrt{\Delta^2+(y_{b/f}+d_{\theta_k})^2}\right]y_{b/f}}^{W(y_{b/f})}}{\sqrt{\Delta^2+(1+\tan^2(\theta_k))(y_{b/f}+d_{\theta_k})^2/\cos(\theta_k)}} - k_x x_{b/f}^2\end{aligned} \tag{26}$$

The $\dot{V}$ equation has two terms. First: $-k_x x_{b/f}^2$ which is always $\leqslant 0$, and a second one where the the denominator is always positive, since Condition (1) restricts $\cos(\theta_k)$ to always be positive in the range of $\theta_k$. Therefore, showing that the numerator which we call $W(y_{b/f})$ has one unique solution of $W(y_{b/f}) = 0$ at $y_{b/f} = 0$ and that this solution is also a maximum, will show that $\dot{V}$ is negative definite:

$$\begin{aligned}&W(y_{b/f}) = -U\left[\tan(\theta_{\max})(y_{b/f}+d_{\theta_k})-\tan(\theta_k)\sqrt{\Delta^2+(y_{b/f}+d_{\theta_k})^2}\right]y_{b/f} \\ &W(y_{b/f}) = 0:\ y_{b/f} = 0\end{aligned} \tag{27}$$

By taking the first and second derivative of $W(y_{b/f})$ it can be seen that $y_{b/f} = 0$ is a maximum value of W:

$$\begin{aligned}&W'(0) = 0 \\ &W''(0) = -2U\tan(\theta_{\max})\left[1-\frac{\tan^2(\theta_k)}{\tan^2(\theta_{\max})}\right] < 0\end{aligned} \tag{28}$$

Therefore $\dot{V} \leqslant 0$ is bounded by:

$$\dot{V} \leqslant \frac{-U_{\min}\left[\tan(\theta_{\max})(y_{b/f}+d_{\theta_k})-\tan(\theta_k)\sqrt{\Delta^2+(y_{b/f}+d_{\theta_k})^2}\right]y_{b/f}}{\sqrt{\Delta^2+(1+\tan^2(\theta_k))(y_{b/f}+d_{\theta_k})^2/\cos(\theta_k)}} - k_x x_{b/f}^2 \tag{29}$$

$\dot{V}$ is shown to be negative definite and thus the nominal system is UGAS. Theorem 1 from Sontag (1989) can now be applied to prove stability of the entire cascaded system. In particular, the nominal system is UGAS with a quadratic Lyapunov-function. The perturbing error dynamics are UGES, and the interconnection matrix $\boldsymbol{H}(U,\boldsymbol{\xi})$

$$\begin{aligned}\dot{y}_{b/f} &= u\sin(\psi_{b/f}) + v\cos(\psi_{b/f}) - \dot{s}\kappa\ x_{b/f}\dot{y}_{b/f} = \cos(\theta_k)(-u\sin(\alpha)+v\cos(\alpha)) - \sin(\theta_k)(u\cos(\alpha)+v\sin(\alpha)) - \dot{s}\kappa\ x_{b/f} + \\ &+ \cos(\theta_k)\tilde{\psi}\left[\frac{\cos(\tilde{\psi})-1}{\tilde{\psi}}(v\cos(\alpha)-u\sin(\alpha)) + \frac{\sin(\tilde{\psi})}{\tilde{\psi}}(u\cos(\alpha)+v\sin(\alpha))\right] + \sin(\theta_k)\tilde{\psi}\left[\frac{\cos(\tilde{\psi})-1}{\tilde{\psi}}(-u\cos(\alpha)-v\sin(\alpha)) + \frac{\sin(\tilde{\psi})}{\tilde{\psi}}(-u\sin(\alpha)+v\cos(\alpha))\right]\end{aligned} \tag{22}$$

$$\begin{aligned}\dot{y}_{b/f} &= -U\frac{\tan(\theta_{\max})(y_{b/f}+d_{\theta_k})-\tan(\theta_k)\sqrt{\Delta^2+(y_{b/f}+d_{\theta_k})^2}}{\sqrt{\Delta^2+(1+\tan^2(\theta_{\max}))(y_{b/f}+d_{\theta_k})^2/\cos(\theta_k)}} - \dot{s}\kappa\ x_{b/f} + \\ &\underbrace{\tilde{\psi}\left[\frac{\sin(\tilde{\psi})}{\tilde{\psi}}U\frac{-\sin(\theta_k)\tan(\theta_k)(y_{b/f}+d_{\theta_k})+\cos(\theta_k)\sqrt{\Delta^2+(y_{b/f}+d_{\theta_k})^2}}{\sqrt{\Delta^2+(1+\tan^2(\theta_{\max}))(y_{b/f}+d_{\theta_k})^2}} - \frac{\cos(\tilde{\psi})-1}{\tilde{\psi}}U\frac{\cos(\theta_k)\tan(\theta_k)(y_{b/f}+d_{\theta_k})-sin(\theta_k)\sqrt{\Delta^2+(y_{b/f}+d_{\theta_k})^2}}{\sqrt{\Delta^2+(1+\tan^2(\theta_{\max}))(y_{b/f}+d_{\theta_k})^2}}\right]}_{\triangleq h(U,\boldsymbol{\xi})}\end{aligned} \tag{23}$$

is globally bounded under Assumption 2 which guarantees that U is bounded by $U \leqslant \sqrt{u_{\max}^2 + v_{\max}^2}$. Consequently, the cascaded system in (24) and (18) is UGAS, and $x_{b/f}, x_{b/f}$ converge to zero with uniform global asymptotic stability. Thus the control objectives (12) are satisfied.

## 6. SIMULATIONS

The effectiveness of the control strategy will be tested using two different scenarios.

A) A ground vehicle with no side slip.
B) An underwater vehicle with side slip.

For both cases, the lack of a global positioning system is assumed to be the reason for using alternative positioning sources. Also, in each scenario the vehicle starts from two different regions close to the path; The first "outside" (highlighted in blue in Fig. 2) the spiral, where the path will always be between the vehicle and target (▲). In the second scenario the vehicle starts "inside" the spiral. In this case during the steering towards the path the vehicle must take a trajectory in which view of the target (▲) is closer to the FOV limits.

Note: If two new spirals were created from both regions starting positions (*in* and *out*) to the end point $p_{k+1}$, then the bearing angles $\theta_k$ of these paths would be: $\theta_{k_{out}} < \theta_k < \theta_{k_{in}}$.

For both cases the vehicle will have a visual restriction of $\theta_{\max} = \frac{\pi}{3}$ and start with a yaw angle that points directly at the transponder/landmark (▲), i.e. $\theta = 0$. Both cases also will have a logarithmic spiral with the same bearing $\theta_k$, but in different proportions according to their maneuvering characteristics.

### 6.1 Ground Vehicle

We first consider a ground robot with zero side-slip angles which obtains its navigation information by observing a visual landmark (▲) on the ground. The model used in this paper is described in Fierro and Lewis (1995), which describes the dynamics of a robot with two driving wheels mounted on the same axis, and a free front wheel. Our study case in particular has the body-fixed coordinate system at the center of the axis.

$$\begin{aligned} \dot{\boldsymbol{q}} &= \boldsymbol{S}(\psi)\boldsymbol{v} \\ \boldsymbol{M}\dot{\boldsymbol{v}} + \boldsymbol{F}(\boldsymbol{v}) &= \boldsymbol{B}(\psi)\boldsymbol{\tau} \end{aligned} \tag{30}$$

The vector $\boldsymbol{F}(\boldsymbol{v})$ contains the surface friction forces, and $\tau$ contains a vector with the force applied to each wheel.

$$\boldsymbol{S} \triangleq \begin{bmatrix} \cos(\psi) & 0 \\ \sin(\psi) & 0 \\ 0 & 1 \end{bmatrix}, \boldsymbol{M} \triangleq \begin{bmatrix} m & 0 & 0 \\ 0 & m & 0 \\ 0 & 0 & I \end{bmatrix}, \boldsymbol{B} \triangleq \frac{1}{r}\begin{bmatrix} \cos(\psi) & \cos(\psi) \\ \sin(\psi) & \sin(\psi) \\ R & -R \end{bmatrix} \tag{31}$$

The ground vehicle is required to follow a path $\mathcal{P}$ described by point $P_1 : [100, 0]$ to a point $P_2 : [25, \frac{\pi}{2}]$, from the inside starting point $P_{0_{In}} : [95, 0]$ and the outside $P_{0_{Out}} : [100, \frac{\pi}{36}]$, respectively. For this case the parameters of the guidance control law were tuned to: $\Delta = 3, k_p = 0.2, k_d = 2$.

### 6.2 Marine Vehicle

In the second scenario a underwater vehicle, which receives both range and bearing from a single transponder. The dynamic model of Fossen (2011) is used. The vehicle is required to follow the path $\mathcal{P}$ described by point $P_1 : [600, 0]$ to a point $P_2 : [150, \frac{\pi}{2}]$. Starting from the inside position: $P_{0_{In}} : [580, 0]$ and the outside $P_{0_{Out}} : [600, \frac{\pi}{36}]$. For this case the parameters of the guidance control law were tuned to: $\Delta = 40, k_p = 2, k_d = 60$;

$$\begin{aligned} \dot{\boldsymbol{\eta}} &= \boldsymbol{R}(\psi)\boldsymbol{v} \\ \boldsymbol{M}\dot{\boldsymbol{v}} + \boldsymbol{C}(\boldsymbol{v})\boldsymbol{v} + \boldsymbol{D}\boldsymbol{v} &= \boldsymbol{B}\boldsymbol{f} \end{aligned} \tag{32}$$

The vector $\boldsymbol{f}$ contains the control inputs, i.e. the rudder angle $\delta$ and the surge force $\tau$.

$$\begin{aligned} &\boldsymbol{M} \triangleq \begin{bmatrix} m_{11} & 0 & 0 \\ 0 & m_{22} & m_{23} \\ 0 & m_{32} & m_{33} \end{bmatrix}, \boldsymbol{D} \triangleq \begin{bmatrix} d_{11} & 0 & 0 \\ 0 & d_{22} & d_{23} \\ 0 & d_{32} & d_{33} \end{bmatrix} \\ &\boldsymbol{B} \triangleq \begin{bmatrix} b_{11} & 0 \\ 0 & b_{22} \\ 0 & b_{32} \end{bmatrix}, \boldsymbol{C}(\boldsymbol{v}) \triangleq \begin{bmatrix} 0 & 0 & -m_{22}v - v_{23}r \\ 0 & 0 & m_{11}u \\ m_{22}v + m_{23}r & m_{11}u & 0 \end{bmatrix} \end{aligned} \tag{33}$$

The coefficients of the matrices $\boldsymbol{M}, \boldsymbol{D}, \boldsymbol{B}, \boldsymbol{C}$ were extracted from Healey and Lienard (1993).

### 6.3 Discussion

The results of the simulations are shown in Fig. 5-10. The trajectory of the vehicle while approaching to the path for the two different scenarios is shown in Fig.5,6. The vehicles converge to the path in all the cases. The figures also show that the "inside" trajectory takes longer to converge than the "outside" trajectory. This is an expected result because the steering capability becomes restricted by the FOV limits.

Fig. 7 and Fig. 8 show the time evolution of the bearing angle w.r.t. the landmark (▲). The shaded area represents the FOV. For both vehicles, the desired angle (dotted-red) of the "inside" trajectory remains close to $\theta_{\max}$ (steps 1-2). This is due to the restriction that the guidance law imposes to preserve FOV, making the vehicle converge slower in comparison with the "outside" trajectory (dotted-blue), where the vehicle is allowed to turn faster towards the path, since turning towards the path entails turning towards the landmark.

The effect of the side-slip angle can be observed in the desired angle ("outside"/dotted red) of the underwater vehicle. It creates an overshoot, almost reaching the limits of FOV ($\theta_{\max}$). On the other hand, this overshoot does not happen for the ground vehicle, in which the desired angle gradually approaches to $\theta_k$.

For this reason, the ground vehicle can be tuned with a smaller $\Delta$, allowing it to reach the path much faster than the underwater vehicle. This can be seen in Fig. 9 and Fig. 10 which show the distance to the path. The "outside"(blue) trajectory converges notably faster for the ground vehicle. However, this is not the case for the "inside"(red) trajectory, mainly because the FOV is limiting how fast it can converge to the path.

Finally, for the "inside"(red) trajectory, it can be seen that both vehicles drift away from the path at the beginning. The vehicles start with a bearing angle that points away from the path and they do not start converging until the bearing has been adjusted. For the "outside"(blue) trajectory the bearing points towards the path which makes the vehicle converge since the beginning.

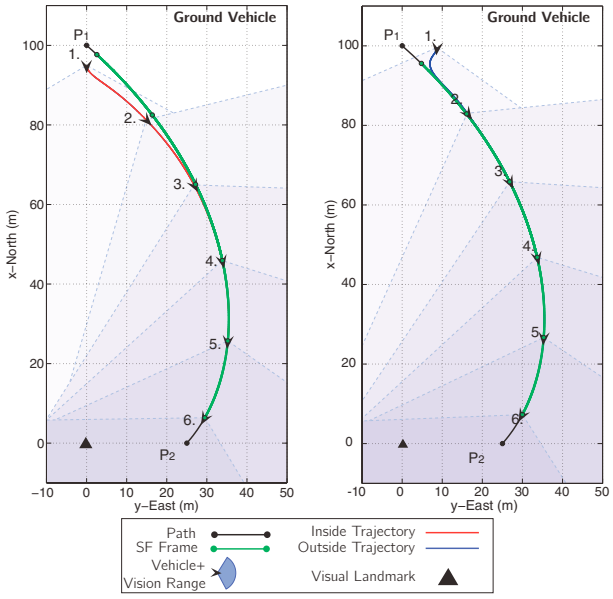


Fig. 5. The trajectory of the ground vehicle. In the left plot the vehicle starts at the "inside", while the right plot shows the trajectory starting from the "outside". The shaded areas represent the FOV at each sample (1-6).

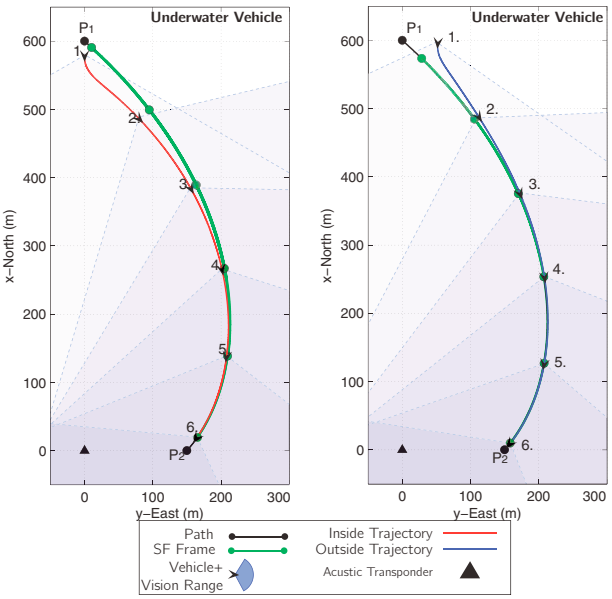


Fig. 6. The trajectory of the underwater vehicle. In the left plot the vehicle starts at the "inside", while the right plot shows the trajectory starting from the "outside". The shaded areas represent the FOV.

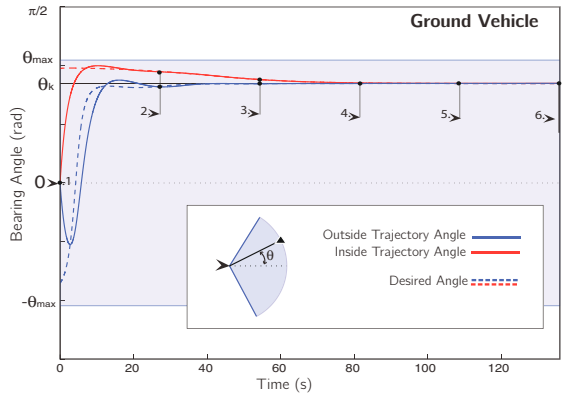


Fig. 7. The bearing angle $\theta$ w.r.t. the landmark (▲). The shaded area represents the limits of vision.

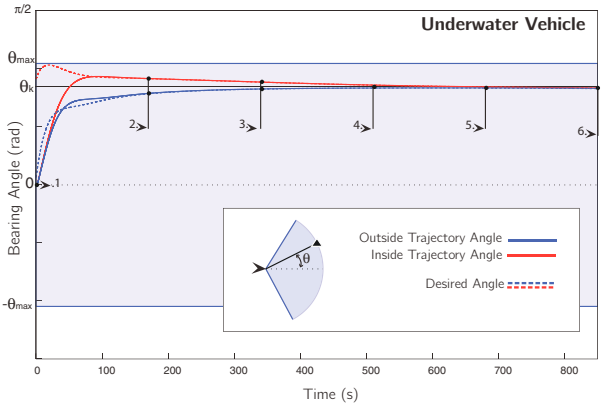


Fig. 8. The bearing angle $\theta$ w.r.t. the transponder (▲). The shaded area represents the limits of vision.

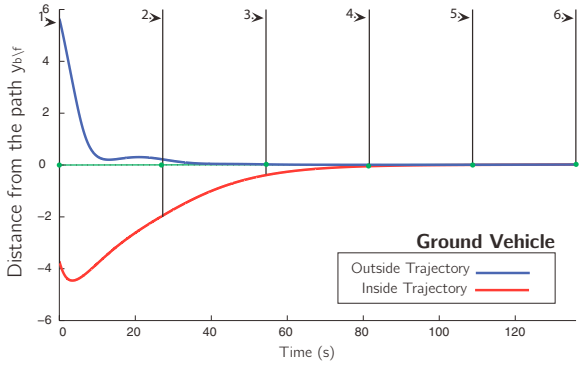


Fig. 9. The time evolution of the distance to the path $y_{b/f}$ for the ground vehicle case during time

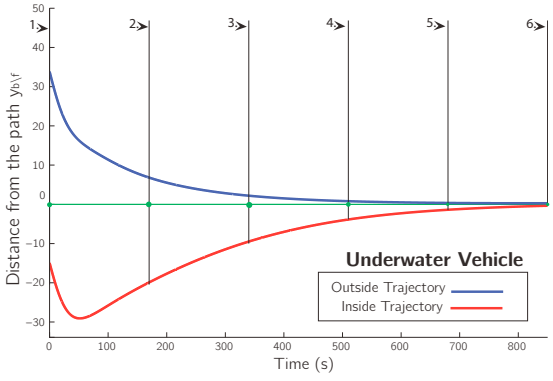


Fig. 10. The time evolution of the distance to the path $y_{b/f}$ for the underwater vehicle case during time

## 7. CONCLUSIONS

In this paper we have shown the benefits of using logarithmic spirals paths for motion planning purposes of underactuated vehicles that have a limited FOV. We have proposed the description of a path that connects two points, in which a vehicle moving along this path will preserve the FOV of the given landmark/transponder.

A guidance and control system for a large class of underactuated vehicles is developed to solve the control objective of making the vehicle steer towards and follow the spiral path and at the same time preserve the vision of a transponder/landmark. This paper proves the convergence to the desired path with asymptotic stability. A simulation study confirms the theoretical results.

Future work will include other larger classes of spirals and considerations on the effects of ocean currents/drag forces.

## REFERENCES


Bhattacharya, S., Murrieta-Cid, R., and Hutchinson, S. (2007). Optimal paths for landmark-based navigation by differential-drive vehicles with field-of-view constraints. *IEEE Transactions on Robotics*, (1), 47–59.

Børhaug, E. and Pettersen, K. (2006). LOS path following for underactuated underwater vehicle. In *Proc. 7th IFAC Conference on Manoeuvring and Control of Marine Craft*. San Diego,CA.

Boyadzhiev, K.N. (1999). Spirals and conchospirals in the flight of insects. *College Mathematics Journal*, 30, 23–31.

Breivik, M., Fossen, T., et al. (2008). Guidance laws for planar motion control. In *47th IEEE Conference on Decision and Control, 2008.*, 570–577. Cancun, Mexico.

Encarnaçao, P. and Pascoal, A. (2000). 3D path following for autonomous underwater vehicle. In *Proc. 39 th IEEE Conference on Decision and Control*. Sydney, Australia.

Fierro, R. and Lewis, F.L. (1995). Control of a nonholonomic mobile robot: backstepping kinematics into dynamics. In *Proc. 34th IEEE Conference on Decision and Control, 1995.*, 3805–3810. New Orelans, LA.

Fossen, T., Pettersen, K.Y., Galeazzi, R., et al. (2015). Line-of-sight path following for dubins paths with adaptive sideslip compensation of drift forces. *IEEE Transactions on Control Systems Technology*, (2), 820–827.

Fossen, T.I. (2011). *Handbook of marine craft hydrodynamics and motion control*. John Wiley & Sons.

Healey, A.J. and Lienard, D. (1993). Multivariable sliding mode control for autonomous diving and steering of unmanned underwater vehicles. *IEEE Journal of Oceanic Engineering*, 18(3), 327–339.

López-Nicolás, G., Gans, N.R., Bhattacharya, S., Sagüés, C., Guerrero, J.J., and Hutchinson, S. (2010). Homography-based control scheme for mobile robots with nonholonomic and field-of-view constraints. *IEEE Transactions on Cybernetics, Systems, Man, and Cybernetics*, (4), 1115–1127.

Maniatopoulos, S., Panagou, D., and Kyriakopoulos, K.J. (2013). Model predictive control for the navigation of a nonholonomic vehicle with field-of-view constraints. In *American Control Conference (ACC), 2013*, 3967–3972.

Moe, S., Caharija, W., Pettersen, K.Y., and Schjolberg, I. (2014). Path following of underactuated marine surface vessels in the presence of unknown ocean currents. In *Proc. American Control Conference (ACC) 2014*, 3856–3861. Portland,OR.

Papoulias, F.A. (1991). Bifurcation analysis of line of sight vehicle guidance using sliding modes. *International Journal of Bifurcation and Chaos*, 1(04), 849–865.

Reeds, J. and Shepp, L. (1990). Optimal paths for a car that goes both forwards and backwards. *Pacific journal of mathematics*, 145(2), 367–393.

Rysdyk, R. (2006). Unmanned aerial vehicle path following for target observation in wind. *Journal of guidance, control, and dynamics*, (5), 1092–1100.

Salaris, P., Fontanelli, D., Pallottino, L., and Bicchi, A. (2010). Shortest paths for a robot with nonholonomic and field-of-view constraints. *IEEE Transactions on Robotics*, (2), 269–281.

Salaris, P., Pallottino, L., and Bicchi, A. (2012). Shortest paths for finned, winged, legged, and wheeled vehicles with side-looking sensors. *The International Journal of Robotics Research*, (8), 997–1017.

Salaris, P., Pallottino, L., Hutchinson, S., and Bicchi, A. (2011). From optimal planning to visual servoing with limited FOV. In *IEEE/RSJ International Conference on Intelligent Robots and Systems (IROS), 2011*, 2817–2824.

Sontag, E. (1989). Remarks on stabilization and input-to-state stability. In *Proc. 28th IEEE Conference on Decision and Control*. Tampa, FL.

Stolle, S. and Rysdyk, R. (2003). Flight path following guidance for unmanned air vehicles with pan-tilt camera for target observation. In *Proc. 22nd Digital Avionics Systems Conference, 2003.* Indianapolis, IN.

Tucker, V.A. (2000). The deep fovea, sideways vision and spiral flight paths in raptors. *Journal of Experimental Biology*, (24), 3745–3754.